J. KSIAM Vol.15, No.1, 67-82, 2011

AN ACCURATE AND EFFICIENT CALCULATION OF HIGH ENTHALPY FLOWS USING A HIGH ORDER NEW LIMITING PROCESS

SUNGJUN NOH[1], KYUNG ROCK LEE[1], JUNG HO PARK[1] AND KYU HONG KIM[1†]

[1]DEPARTMENT OF MECHANICAL AND AEROSPACE ENGINEERING, SEOUL NATIONAL UNIVERSITY, SOUTH KOREA
E-mail address: dykmis@snu.ac.kr, rudfhr1228@hotmail.com, ultimatepark@hanmail.net, aerocfd1@snu.ac.kr

ABSTRACT. Calculation of accurate wall heat flux for high enthalpy flows requires a dense grid system, which leads to significantly large computational time. A high-order scheme can improve the efficiency of calculation because wall heat flux can be obtained accurately even with a relatively coarse grid system. However, conventional high order schemes have some drawbacks such as oscillations near a discontinuity and instability in multi-dimensional problem. To resolve these problems, enhanced Multi-dimensional Limiting Process(e-MLP) was applied as a high-order scheme. It could provide robust and accurate solutions with high order accuracy in calculation of high enthalpy flows within a short time. We could confirm the efficiency of the high order e-MLP scheme through grid convergence tests with different grid densities in a hypersonic blunt nose problem.

1. INTRODUCTION

In simulation of a hypersonic and high temperature flow including an ablation at the wall surface, an accurate prediction of wall heat flux is essential. In a hypersonic flow, the large amount of kinetic energy of free-stream is converted to thermal energy, which generates high temperature gradient near the wall. Thus, the temperature gradient has to be calculated accurately to obtain exact wall heat flux, and those calculations demand a dense grid system. Also, in case that an ablation occurs at the wall, many cases should be calculated to consider the change of surface conditions as time goes on, i.e., it takes a lot of computation time. To decrease the computation time, an efficient calculation in each case is required. Until now, 2^{nd} order schemes have been widely used for calculation of the hypersonic flow. However, in case when the wall heat flux is very high, grid points should be clustered very densely enough to restrict a time step severely. Consequently, overall computing time increases tremendously. To overcome this situation, a high order scheme is suggested as one of the solutions. It can provide an accurate solution even when a coarse grid system is used. However, high order computations for flow including shock waves always induce unnecessary numerical oscillations near the discontinuity. Especially, for a strong shock wave, those oscillations are amplified and finally make the whole computation fail. For that reason, many studies have been carried out to remove the numerical oscillations. The

Received by the editors March 22, 2011; Revised March 23, 2011..
2000 *Mathematics Subject Classification*. 93B05.
Key words and phrases. High enthalpy flow.
† Corresponding author.

notable results are Total Variation Diminishing (TVD) [1-2], Essentially Non-Oscillatory (ENO) [3], Total Variation Bounded (TVB) [4] and Multi-dimensional Limiting Process (MLP) [5, 7]. Although many researchers have much effort to study on a limiting function, there is no perfect limiter for oscillation removal in a shock discontinuity of multi-dimensions until now. First, TVD and ENO schemes are developed based on mathematical analyses of the one-dimensional scalar convection equation, so they result in undershoot or overshoot when solving a multi-dimensional problem. Also conventional TVD criterion is somewhat unsatisfactory near extrema due to clipping phenomena. Although ENO scheme avoided unphysical clipping at extrema, it has low accuracy.

MLP gives the stable result around the shock wave in multi-dimensional problems by giving property distribution within the maximum and minimum values of the neighboring cells around the cell interface. However, MLP is not suitable for a continuous region, because it gives excessive damping for local extrema in a continuous region. To solve this problem, a distinguishing criterion which determines whether a computational region is discontinuous or not is introduced in MLP. As a result, MLP limiter is only applied to a discontinuous region [8]. However, it has also deficiency in a linear discontinuous region, which gives relatively diffusive results. For effective oscillation removal, a discontinuous region has to be thoroughly distinguished and the information about the region needs to be considered in a flux schemes as well as a high order interpolation scheme. Therefore, an oscillation about the region needs to be considered in a flux schemes as well as a high order interpolation scheme. To sum up, an oscillation removal process should have 2 features. The first feature is separation of discontinuity search routine from high order interpolation. And the second feature is consideration of real flow physics in discontinuity search routine.

Consequently, a new approach involving a multi-dimensional high order scheme based on the Multi-dimensional Limiting Process (MLP) is introduced. It is termed as “Enhanced Multi-dimensional Limiting Process” (e-MLP) [6]. With the use of new method, the accuracy of the solution is increased and the computation becomes robust against shock instability. Moreover, the computational cost is reduced because a limiting function is applied only to a discontinuous region.

This paper is organized as follows. After the description of the governing equations, numerical schemes including e-MLP are described. We performed the computation about basic 1-D shock/sine interactive problem to check the enhancement e-MLP, and hypersonic blunt nose problem in high enthalpy flow to verify the efficiency increment of high order scheme using e-MLP.

2. GOVERNING EQUATIONS

2.1. **Governing equations**

2D axi-symmetric Navier-Stokes equations including chemical reactions are described as follows. All terms are represented in vector form, and the bottom terms in each vector are about chemical reactions. Subscript v means viscous term, and vector S is species term. In axi-symmetric case, α equals 1.

$$\frac{\partial \mathbf{Q}}{\partial \mathrm{t}}+\frac{\partial \mathbf{E}}{\partial \mathrm{x}}+\frac{\partial \mathbf{F}}{\partial \mathrm{y}}=\frac{\partial \mathbf{E}_v}{\partial \mathrm{x}}+\frac{\partial \mathbf{F}_v}{\partial \mathrm{y}}+\mathbf{S}+\alpha(\mathbf{H}_v-\mathbf{H}) \tag{1}$$

$$\mathbf{Q}=\begin{pmatrix}\rho\\ \rho u\\ \rho v\\ \rho e_t\\ \rho_i\\ \mathrm{M}\\ \sum_i \rho e_{vib,i}\end{pmatrix},\quad \mathbf{E}=\begin{pmatrix}\rho u\\ \rho u^2+p\\ \rho uv\\ (\rho e_t+p)u\\ \rho_i u\\ \mathrm{M}\\ \sum_i \rho e_{vib,i}u\end{pmatrix},\quad \mathbf{F}=\begin{pmatrix}\rho v\\ \rho uv\\ \rho v^2+p\\ (\rho e_t+p)v\\ \rho_i v\\ \mathrm{M}\\ \sum_i \rho e_{vib,i}v\end{pmatrix},\quad \mathbf{S}=\begin{pmatrix}0\\ 0\\ 0\\ 0\\ W_i\\ \mathrm{M}\\ \sum_i W_{vib},i\end{pmatrix} \tag{2}$$

$$\mathbf{E}_v=\begin{pmatrix}0\\ \frac{M_\infty}{\mathrm{Re}_\infty}\tau_{xx}\\ \frac{M_\infty}{\mathrm{Re}_\infty}\tau_{xy}\\ -\frac{M_\infty}{\mathrm{Re}_\infty}\frac{1}{\mathrm{Pr}_\infty(\gamma_\infty-1)}(q_x+\sum_i q_{vx,i})+\frac{M_\infty}{\mathrm{Re}_\infty}(\tau_{xx}u+\tau_{xy}v)+\frac{M_\infty}{\mathrm{Re}_\infty}\sum_i(\rho D_i\frac{\partial c_i}{\partial x})\\ \frac{M_\infty}{\mathrm{Re}_\infty}\rho D_i\frac{\partial c_i}{\partial x}\\ \mathrm{M}\\ \frac{M_\infty}{\mathrm{Re}_\infty}\sum_i \rho e_{vib,i}D_i\frac{\partial c_i}{\partial x}-\frac{M_\infty}{\mathrm{Re}_\infty}\frac{1}{\mathrm{Pr}_\infty(\gamma_\infty-1)}\sum_i q_{vx,i}\end{pmatrix} \tag{3}$$

$$\mathbf{F}_v=\begin{pmatrix}0\\ \frac{M_\infty}{\mathrm{Re}_\infty}\tau_{xy}\\ \frac{M_\infty}{\mathrm{Re}_\infty}\tau_{yy}\\ -\frac{M_\infty}{\mathrm{Re}_\infty}\frac{1}{\mathrm{Pr}_\infty(\gamma_\infty-1)}(q_y+\sum_i q_{vy,i})+\frac{M_\infty}{\mathrm{Re}_\infty}(\tau_{xy}u+\tau_{yy}v)+\frac{M_\infty}{\mathrm{Re}_\infty}\sum_i(\rho D_i\frac{\partial c_i}{\partial y})\\ \frac{M_\infty}{\mathrm{Re}_\infty}\rho D_i\frac{\partial c_i}{\partial y}\\ \mathrm{M}\\ \frac{M_\infty}{\mathrm{Re}_\infty}\sum_i \rho e_{vib,i}D_i\frac{\partial c_i}{\partial y}-\frac{M_\infty}{\mathrm{Re}_\infty}\frac{1}{\mathrm{Pr}_\infty(\gamma_\infty-1)}\sum_i q_{vy,i}\end{pmatrix} \tag{4}$$

$$\mathbf{H} = \frac{1}{y}\begin{pmatrix} \rho u \\ \rho uv \\ \rho v^2 \\ \rho H \\ \rho_i v \\ \text{M} \\ \sum_i \rho e_{vib,i} v \end{pmatrix}, \quad \mathbf{H}_v = \frac{1}{y}\begin{pmatrix} 0 \\ \tau_{xy} - \frac{2}{3} y \frac{\partial}{\partial x}(\mu \frac{v}{y}) \\ \tau_{yy} - \tau_{\theta\theta} - \frac{2}{3}(\mu \frac{v}{y}) - \frac{2}{3} y \frac{\partial}{\partial y}(\mu \frac{v}{y}) \\ u\tau_{xx} + v\tau_{yy} - q_y - \frac{2}{3}(\mu \frac{v^2}{y}) - \frac{2}{3} y \frac{\partial}{\partial y}(\mu \frac{v^2}{y}) - \frac{2}{3} y \frac{\partial}{\partial x}(\mu \frac{uv}{y}) \\ \rho D_i \frac{\partial c_i}{\partial y} \\ \text{M} \\ \sum_i \rho \varepsilon_{v,i}(T_{v,i}) D_i \frac{\partial c_i}{\partial y} \end{pmatrix} \tag{5}$$

2.2. **Wall Boundary Conditions**

The boundary condition at the wall surface is a finite catalytic wall condition. At the high temperature, four types of chemical reaction generally occur at the carbon ablator: oxidation, nitration, catalytic recombination and sublimation. Each chemical reaction equations are as follows.

Oxidation

$$O + C(c) \rightarrow CO + 3.61 \times 10^5 J/mol$$

Nitration

$$N + C(c) \rightarrow CN + 3.40 \times 10^4 J/mol$$

Catalytic recombination

$$O + O \leftrightarrow O_2 + 4.94 \times 10^5 J/mol$$
$$N + N \leftrightarrow N_2 + 9.45 \times 10^5 J/mol$$
$$NO + NO \leftrightarrow N_2 + O_2 + 1.81 \times 10^5 J/mol$$

Sublimation

$$C(c) \rightarrow C_2 - 8.29 \times 10^5 J/mol$$
$$C(c) \rightarrow C_3 - 8.11 \times 10^5 J/mol$$

3. NUMERICAL SCHEMES

3.1. **Enhanced Multi-dimensional Limiting Process**

The concept of e-MLP is divided into three steps. First step is a distinguishing step which is introduced to a solver. In this step, the computational domain is divided into continuous, linear discontinuous and nonlinear discontinuous regions. Second step contains enhanced limiting process based on the regional information. In a continuous region, there is no limiting process. In a linear discontinuous region such as a region of contact discontinuity, the conventional TVD criterion is applied. In a nonlinear discontinuous region, MLP limiter is used. In third step, the regional information is fed into a flux scheme as well as a high order interpolation scheme. Based on this information, proper numerical dissipation is added to a nonlinear discontinuous region.

Using these 3 steps, e-MLP can improve the solver in terms of accuracy, robustness and efficiency as follows. First, the switching of the limiting criteria in e-MLP can enhance the accuracy of solutions. Limiting criteria is selected according to the 3 features of the flow field. In a continuous region, no limiting function is used because there are no clipping phenomena. In a linear discontinuous region, the conventional TVD criterion is used to avoid excessive damping. In a nonlinear discontinuous region, the MLP limiter is used in order to remove oscillation around the discontinuities. As a result, e-MLP can include a considerable amount of information pertaining to flow physics and can provide accurate solutions with the enhanced oscillation removal ability, especially in the event of a complex shock structure.

Second, e-MLP is very robust against shock instability due to the multi-dimensional search routine for discontinuities. Through the search of discontinuities in e-MLP, proper numerical dissipation is added in a flux evaluation scheme. In a conventional one-dimensional discontinuity searching, the existence of shock wave is determined one-dimensionally, which can cause a density perturbation that acts as a source of instability in the numerical shock region and leads to bad convergence in a steady problem. However, e-MLP damps out the perturbation by help of the independent multi-dimensional search routine for discontinuities.

Third, e-MLP improves the efficiency comparing to the conventional methods through the distinguishing regions. Generally, the majority of a computational domain is a smooth region with the exception of some discontinuous regions, where limiting criteria are necessary. In this situation, the application of a limiting function to the entire domain is a waste of computational resources. Therefore, the overall computation time is reduced by application of limiting criteria only in a discontinuous region.

3.2. **Process of E-MLP**

The overall process of e-MLP is listed in Fig. 1. The process is divided into 4 steps. Each step is briefly explained below.

Distinction of the computational domain

For accurate distinction between continuous, linear discontinuous and nonlinear discontinuous regions, each type of region is searched multi-dimensionally by using the 4th order of polynomial interpolation and Gibbs phenomenon.

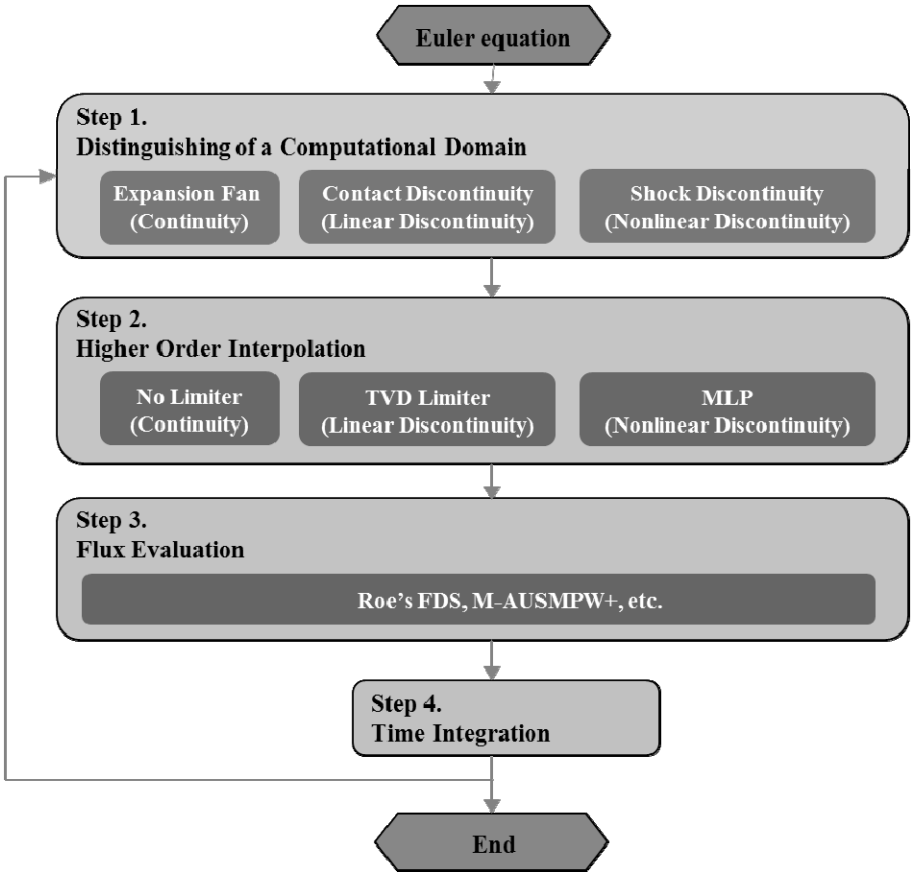

FIGURE 1. Overall Procedure of e-MLP

Higher order interpolation

After the distinguishing step, an appropriate limiting function is applied to each type of region. In a continuous region, a limiting function is unnecessary and simple high order accurate interpolation is performed. In a linear discontinuous region, the conventional TVD criterion is applied for oscillation removal. Last, in a nonlinear discontinuous region, MLP limiter is used.

Flux evaluation

For flux scheme, e-MLP easily cooperates with any numerical scheme such as Roe's FDS [9], AUSMPW+/M-AUSMPW+ [10, 11], etc. In the present paper, M-AUSMPW+ is mainly used as a flux scheme at cell interfaces.

Time integration

In e-MLP, any type of time integration scheme can be applied among implicit or explicit methods. In the present study, the 3rd order of the Runge-Kutta scheme is used for time integration. [12]

Distinguishing Step

Distinguishing between continuous and discontinuous regions is important for effective oscillation removal. However, with conventional limiters such as TVD, TVB, ENO and others, it is not easy to present precise information about a discontinuity to a flux scheme because discontinuity search algorithms of those limiters are generally coupled with an interpolation scheme. Therefore, search routine should be separated from an interpolation scheme to distinguish linear/nonlinear discontinuities multi-dimensionally.

In this paper, computation region is firstly divided into continuous and discontinuous region. And secondly, discontinuous region is separated to linear and nonlinear discontinuity. Detail process is mentioned below.

Distinction between continuities and discontinuities

Generally, it is hard to clearly distinguish between continuity and discontinuity in a numerical computation. Even an actual continuous profile is not seen to be continuous if a mesh size is larger than some threshold value. On the other hand, a numerical discontinuity looks to be a continuous wave if numerical dissipation is so large that the discontinuity is smeared a lot. In this paper, Gibbs phenomenon at the edges of discontinuity is used to define numerical discontinuity because it is definitely necessary to introduce the new definition of numerical discontinuity which is affected by the mesh size. The 4th order of central differencing scheme is selected as the sensing function to indicate whether or not the Gibbs phenomenon occurs from the given distribution. An approximated value $f_{approxi}$ is defined as Eq. (6).

$$f_{approxi,i} = \frac{-f_{i-2} + 4f_{i-1} + 4f_{i+1} - f_{i+2}}{6} = f_i + O(\Delta x^4) \tag{6}$$

In a continuous region, the difference at point i between an original value and an approximated value is derived as Eq. (7).

$$d_i = \frac{\left| f_{approxi,i} - f_i \right|}{\left| f \right|_i} \cong O(\Delta x^4) \tag{7}$$

In a discontinuous region, Gibbs phenomena are easily observed around the edges of numerical discontinuities and the variation d_i is considerably larger than the order of $O(\Delta x^4)$, as in Eq. (8). The difference between original distribution and interpolated value can be seen in Fig. 2.

$$d_i >> O(\Delta x^4) \tag{8}$$

From the result of Fig. 2, it is thought that Gibbs phenomena are good criteria for numerically differentiating a discontinuous region from a continuous region. In this paper, threshold value, ε, is introduced to identify Gibbs phenomena and then define numerically

continuous and discontinuous regions. If $d_i \geq \varepsilon$, it is considered that Gibbs phenomena occur and the current region can be determined as a numerically discontinuous region.

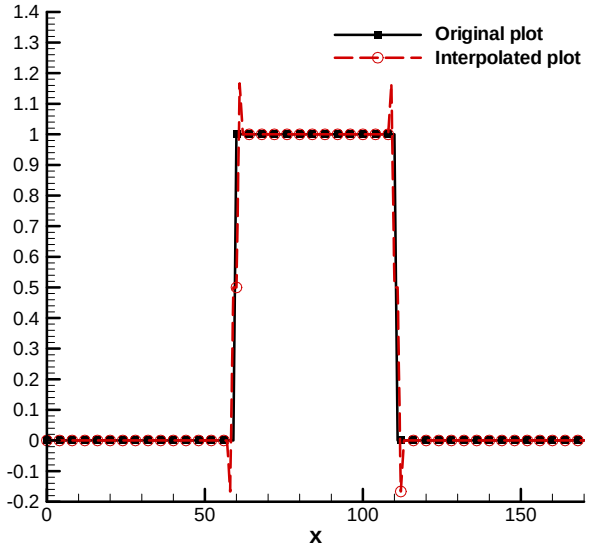

FIGURE 2. An example of Gibbs phenomenon

Distinction between linear and nonlinear discontinuities

For effective oscillation removal in a nonlinear discontinuous region, a strict limiting function is required. While in a nonlinear discontinuous region, excessive damping by a strict limiting function may reduce the accuracy of the solution in a linear discontinuous region. Therefore, the types of discontinuities have to be distinguished properly for appropriate switching of the limiting functions according to the type.

If the inequalities of Eq. (9) are satisfied, a discrete region can be classified as linear contact discontinuity or a slip line. In this paper, the same limiting function is used for both contact discontinuity and slip line because they share the condition that there is no pressure jump across them.

$$d_{\rho,i} = \frac{\left|\rho_{approxi,i} - \rho_i\right|}{\left|\rho_i\right|} > \varepsilon \quad \text{or} \quad d_{u,i} = \frac{\left|u_{approxi,i} - u_i\right|}{\left|u_i\right|} > \varepsilon \text{, and} \quad d_{p,i} = \frac{\left|p_{approxi,i} - p_i\right|}{\left|p_i\right|} \approx O(\Delta x^4) \tag{9}$$

In a nonlinear discontinuity, the inequalities of Eq. (10) are used.

$$d_{\rho,i} = \frac{\left|\rho_{approxi,i} - \rho_i\right|}{\left|\rho_i\right|} > \varepsilon \quad \text{or} \quad d_{u,i} = \frac{\left|u_{approxi,i} - u_i\right|}{\left|u_i\right|} > \varepsilon \text{, and} \quad d_{p,i} = \frac{\left|p_{approxi,i} - p_i\right|}{\left|p_i\right|} > \varepsilon \tag{10}$$

Only if $d_p \geq \varepsilon$, the region is recognized as a nonlinear discontinuous region in the paper. If $\left|u_i\right|$ is physically zero or almost zero, it can be determined as a discontinuous region even though the region is actually a continuous region. In order to avoid this situation, the

region is enforced to be a continuous region if $|u_i|$ is smaller than 10^{-6} in this paper.

By adjusting the check criteria, e-MLP can be extended to various types of physical problems.

Enhanced limiting process

Different limiting functions are used in each three different regions. In a continuous region, no limiting function is recommended to be applied to a continuous region in e-MLP as Eq. (11). The coefficient β is introduced to enable high order computation and explained at the last of this section.

$$\mathbf{\Phi}_L = \overline{\mathbf{\Phi}}_i + 0.5\beta_L \Delta\mathbf{\Phi}_{i-\frac{1}{2}} \tag{11a}$$

$$\mathbf{\Phi}_R = \overline{\mathbf{\Phi}}_{i+1} - 0.5\beta_R \Delta\mathbf{\Phi}_{i+\frac{3}{2}} \tag{11b}$$

In a linear discontinuous region, the application of MLP limiter may make the discontinuity diffusive, which decreased the accuracy of the solution. Thus, the conventional TVD criterion is used for oscillation removal. Brief equations are written below.

$$\mathbf{\Phi}_L = \overline{\mathbf{\Phi}}_i + 0.5\max(0, \min(2\Delta\mathbf{\Phi}_{i+\frac{1}{2}}, 2\Delta\mathbf{\Phi}_{i-\frac{1}{2}}, \beta_L \Delta\mathbf{\Phi}_{i-\frac{1}{2}})) \tag{12a}$$

$$\mathbf{\Phi}_R = \overline{\mathbf{\Phi}}_{i+1} - 0.5\max(0, \min(2\Delta\mathbf{\Phi}_{i+\frac{1}{2}}, 2\Delta\mathbf{\Phi}_{i+\frac{3}{2}}, \beta_R \Delta\mathbf{\Phi}_{i+\frac{3}{2}})) \tag{12b}$$

In a nonlinear discontinuous region, MLP limiter is used for an appropriate oscillation removal in multi-dimensional problems [5, 6]. Brief equations of MLP are as follows.

$$\mathbf{\Phi}_L = \overline{\mathbf{\Phi}}_i + 0.5\max(0, \min(\alpha_L \Delta\mathbf{\Phi}_{i+\frac{1}{2}}, \alpha_L \Delta\mathbf{\Phi}_{i-\frac{1}{2}}, \beta_L \Delta\mathbf{\Phi}_{i-\frac{1}{2}})) \tag{13a}$$

$$\mathbf{\Phi}_R = \overline{\mathbf{\Phi}}_{i+1} - 0.5\max(0, \min(\alpha_R \Delta\mathbf{\Phi}_{i+\frac{1}{2}}, \alpha_R \Delta\mathbf{\Phi}_{i+\frac{3}{2}}, \beta_R \Delta\mathbf{\Phi}_{i+\frac{3}{2}})) \tag{13b}$$

The definitions of $\beta_{L,R}$ for the 3rd order accurate and the 5th order accurate computations are presented in Eq. (14) and Eq. (15), respectively.

$$\beta_L \Delta\mathbf{\Phi}_{i-\frac{1}{2},j} = -\frac{1}{3}\overline{\mathbf{\Phi}}_{i-1,j} - \frac{1}{3}\overline{\mathbf{\Phi}}_{i,j} + \frac{2}{3}\overline{\mathbf{\Phi}}_{i+1,j} \tag{14a}$$

$$\beta_R \Delta\mathbf{\Phi}_{i+\frac{3}{2},j} = \frac{1}{3}\overline{\mathbf{\Phi}}_{i+2,j} + \frac{1}{3}\overline{\mathbf{\Phi}}_{i+1,j} - \frac{2}{3}\overline{\mathbf{\Phi}}_{i,j} \tag{14b}$$

$$\beta_L \Delta\mathbf{\Phi}_{i-\frac{1}{2},j} = \frac{2}{30}\overline{\mathbf{\Phi}}_{i-2,j} - \frac{13}{30}\overline{\mathbf{\Phi}}_{i-1,j} - \frac{13}{30}\overline{\mathbf{\Phi}}_{i,j} + \frac{27}{30}\overline{\mathbf{\Phi}}_{i+1,j} - \frac{3}{30}\overline{\mathbf{\Phi}}_{i+2,j} \tag{15a}$$

$$\beta_R \Delta\mathbf{\Phi}_{i+\frac{3}{2},j} = -\frac{2}{30}\overline{\mathbf{\Phi}}_{i+3,j} + \frac{13}{30}\overline{\mathbf{\Phi}}_{i+2,j} + \frac{13}{30}\overline{\mathbf{\Phi}}_{i+1,j} - \frac{27}{30}\overline{\mathbf{\Phi}}_{i,j} + \frac{3}{30}\overline{\mathbf{\Phi}}_{i-1,j} \tag{15b}$$

Based on the appropriate application of the limiting functions, the oscillation behavior can be effectively removed. Moreover, better efficiency can be obtained because TVD criterion and MLP limiter are applied only to discontinuous regions.

4. NUMERICAL RESULTS

4.1. **1-D shock/sine interactive problem**

The first case has been tested to assess how well the distinguishing process of e-MLP divides the whole computational region into continuous, linear discontinuous and non-linear discontinuous regions. The initial conditions for shock-sine wave interaction problem are given as Eq. (16) [12].

$$\begin{aligned}(\rho,U,p) &= (3.8571,2.6294,10.333) \quad \text{where} \quad 0 \le x \le 1 \\ (\rho,U,p) &= (1+0.2\sin(5(x-5)),0,1) \quad \text{where} \quad 1 \le x \le 10\end{aligned} \tag{16}$$

Since the test case is one-dimensional problem, MLP limiter is the same as the TVD criterion. Thus, the results of MLP5 always followed the typical features of TVD schemes. For comparing the results between MLP5 and e-MLP5, 1000 grid points are used. The reference result was calculated by using 10000 grid points with MLP5 and called as MLP5-dense. For flux evaluation and time integration, M-AUSMPW+ and the 3rd order of Runge-Kutta method were used, individually.

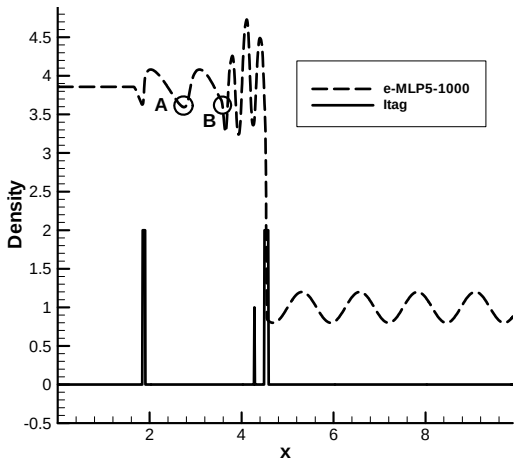

FIGURE 3. Distinguished regions and density contour in shock/sine wave interaction problem

Through the distinguishing process of e-MLP, the most regions were recognized as continuous regions except some discontinuous regions as in Fig. 3. In Fig. 3, Itag represent the distinguished region: 0 for continuous, 1 for linear discontinuous and 2 for nonlinear discontinuous. Detailed density contours of MLP5 and e-MLP5 at t=1sec are shown in Fig.

4. The result of e-MLP5 shows no clipping phenomenon at the extrema, different from that of MLP5. Moreover, the distribution of e-MLP5-1000 is similar to that of MLP5-1600 (MLP5 with 1600 grid points). Because the region around the extrema was determined as a continuous region in e-MLP, no limiter function was applied to the 5th order interpolated value, which could reduce the calculation time as well as increase accuracy.

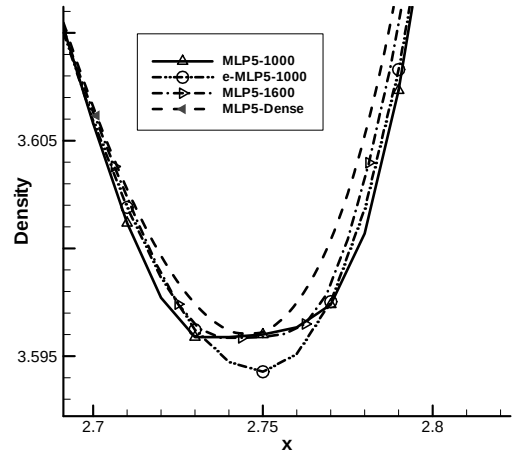

(a) Region A

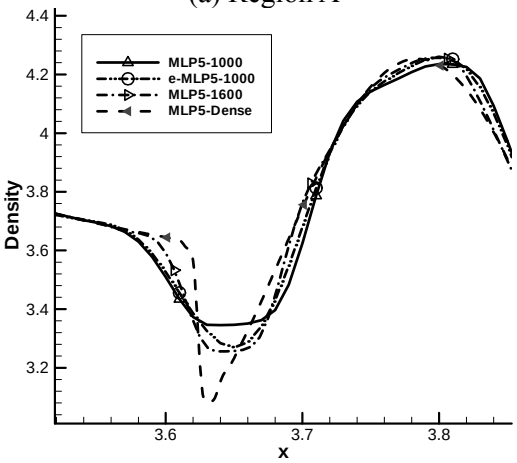

(b) Region B

FIGURE 4. Detailed comparison of density distribution in shock/sine wave interaction problem

4.2. **Grid convergence test on wall heat flux of high enthalpy flow**

In order to investigate the efficiency of the proposed scheme in calculating wall heat flux of high enthalpy flow, we carried out a numerical analysis about hypersonic blunt nose problem.

Test conditions

The free-stream conditions are M_∞=2.0, T_∞=2800K and T_w=1500K. High enthalpy air flows around a hemispheric blunt nose and a bow shock is created in front of the body. As passing through the shock, temperature and pressure are increases and the heat transferred to the wall.

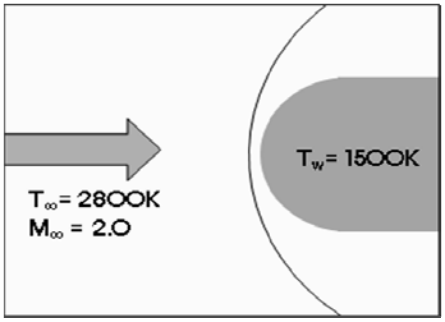

FIGURE 5. Schematics of hypersonic blunt nose problem

For verification of the efficiency of high order set, we carried out a grid convergence test and compared to the result calculated with 2nd order set. Numerical schemes used for the high order set and the 2nd order set are listed in table 1.

TABLE 1. Numerical schemes for the high order set and the second order set

	Viscous flux	Inviscid flux	Boundary
High order set	4^{th} order central differencing	5^{th} order e-MLP	4^{th} order interpolation
2^{nd} order set	2^{nd} order central differencing	2^{nd} order MUSCL	1^{st} order interpolation

In the high order set, viscous flux was calculated with the 4th order central differencing, and the 5th order e-MLP was applied as an interpolation method. Boundary values were calculated with the 4th order interpolation. Meanwhile in the 2nd order scheme, viscous flux was calculated with the 2nd order central differencing and 2nd order MUSCL was used in calculation of inviscid flux. Boundary values were calculated with the linear interpolation.

Commonly, AUSMPW+ was applied as a flux function. Local time stepping method was used and LU-SGS scheme was applied as a time integration scheme.

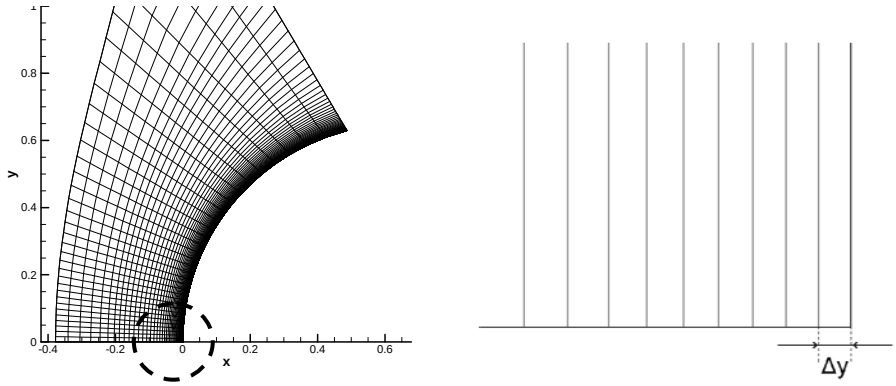

FIGURE 6. Grid system for hypersonic blunt nose problem

In this paper, we tested 5 grid cases which have the same number of grid point (38×100) with the different grid size near the wall as shown in table 2. The grid density was expressed as the ratio of the first mesh size at the stagnation point, Δy , to the radius of blunt body as shown in Fig. 6.

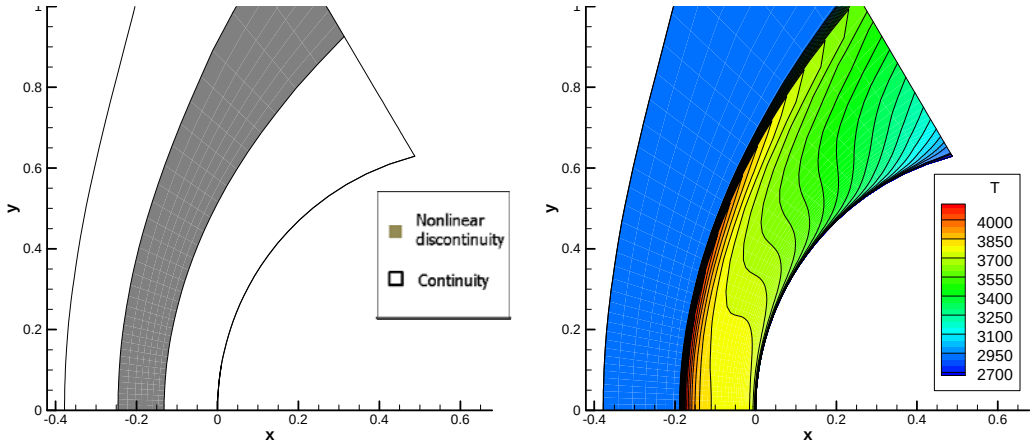

a) Distinguished region b) Temperature contour

FIGURE 7. Distinguished regions and temperature contour

The distinguished regions and temperature contours are shown in Fig. 7. The shock region was well divided as nonlinear discontinuous regions, which verified that the distinguishing process in e-MLP worked successfully. Also, the boundary layer was determined as a continuous region and no limiting function was applied. Therefore, the spatial accuracy was the fully 5th order and the wall heat flux was calculated accurately.

Fig. 8 shows the normalized heat flux at wall for each case. It was normalized to stagnation point value of the high order set with grid 1, which was considered as the converged solution. In the figure, the high order set obtained the converged solution at the

case with grid size of 8.0×10^{-6} (grid 3), while the 2nd order set obtained the converged solution with grid size of 2.0×10^{-6} (grid 1). That is e-MLP calculates the wall heat flux accurately with a coarse grid system. Since e-MLP can use the larger grid size, larger time step is available. The minimum time step for each case is shown in table 1. The minimum time step of the high order scheme with grid 3 is more than 4 times larger than that of 2nd order set with grid 1. Since the larger time step is available for e-MLP scheme, convergence speed is 5 times faster than that of the second order set.

The errors of wall heat flux at the stagnation point compared to the value of the high order set with grid size of 2.0×10^{-6} (grid 1) are listed in table 2. The error of the high order set with grid size of 16.0×10^{-6} (grid 4) is less than the error of the 2nd order set with grid size of 4.0×10^{-6} (grid 2). Similarly, the error of the high order set with grid size of 32.0×10^{-6} (grid 5) is less than the error of the 2nd order set with grid size of 8.0×10^{-6} (grid 3). In other words, we could confirm again that the wall heat flux calculated by the high order set could obtain the converged solution with more than 4 times coarser grid system compared with the 2nd order set.

TABLE 2. Errors of wall heat flux at the stagnation point

	Grid 1	Grid 2	Grid 3	Grid 4	Grid 5
High order set	-	0.01 %	0.08 %	0.22 %	2.29 %
2nd order set	0.15 %	0.89 %	1.57 %	3.91 %	11.6 %

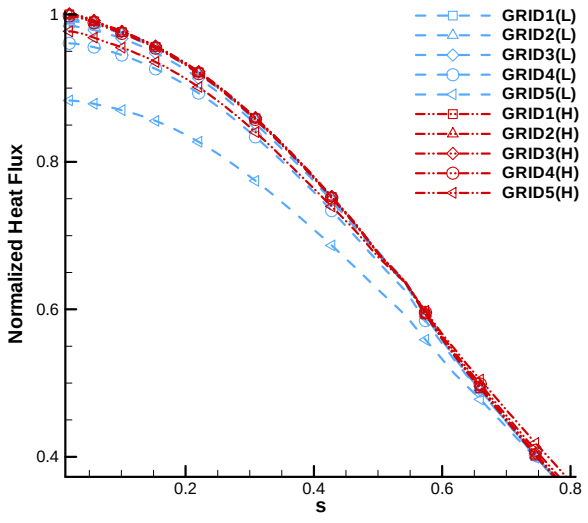

FIGURE 8. Normalized wall heat flux for each case

5. CONCLUSION

For an efficient calculation of high enthalpy flow, the e-MLP was introduced as a high order scheme. The e-MLP scheme has regional distinction process and the computation region is divided in to three regions by multi-dimensional search using Gibbs phenomenon. After regional distinction process, an appropriated limiting function is switched for each region, and presents the regional information to a high order interpolation scheme and a flux scheme. To verify these regional distinction process, calculation about 1-D shock/sine wave interaction problem was performed and confirmed that e-MLP scheme effectively reduced the calculation time as well as increased accuracy.

In order to confirm the efficiency of the high order scheme, a grid convergence test was performed by calculating wall heat flux for various grid densities in the hypersonic blunt nose problem. We compared the minimum time step of the high order set with that of the 2^{nd} order set. Since the large time step is available for e-MLP scheme, the grid converged solution was obtained 5 times faster than the 2^{nd} order set. Also, by comparing errors of each scheme, we could confirm again that the high order set could obtain the converged solution with more than 4 times coarser grid compared to the 2^{nd} order set.

ACKNOWLEDGMENTS

This work was supported by grant KSC-2008-S02-0007 from the Korea Institute of Science and Technology Information and NSL(National Space Lab) program through the National Research Foundation of Korea funded by the Ministry of Education, Science and Technology (20100015076)

REFERENCES

[1] A. Harten, *High Resolution Schemes for Hyperbolic Conservation Laws,* J. Comput. Phys., **49** (1983) 357-393.

[2] P. K. Sweby, *High Resolution Schemes Using Flux Limiters for Hyperbolic Conservation Laws*, SIAM J. Numer. Anal., **21** (1984) 995-1011.

[3] A. Harten, B. Enquist, S. Osher and S. R. Chakravarthy, *Uniformly High Order Accurate Essentially Non-oscillatory Schemes*, III, J. Comput. Phys., **71** (1987) 231-303.

[4] C. W. Shu, *TVB Uniformly High-Order Schemes for Conservation Laws*, Math. Comput., **49** (1987) 105-121.

[5] K. H. Kim, and C. Kim, *Accurate, efficient and monotonic numerical methods for multi-dimensional compressible flows, Part II : Multi-dimensional Limiting Process*, J. Comput. Phys., **208** (2005) 570-615,

[6] H. M. Kang, K. H. Kim and D. H. Lee, *A New Approach of a Limiting Process for Multi-Dimensional Flows*, J. Comput. Phys., **229** (2010) 7102-7128.

[7] S. Yoon, C. Kim, and K. Kim, *Multi-dimensional limiting process for three-dimensional flow physics analyses*. Journal of Computational Physics, **227** (2008), pp. 6001-6043.

[8] S. Kim., S. Lee., and K. Kim, *Wavenumber-extended high-order oscillation control finite volume schemes for multi-dimensional aeroacoustic computations*, Journal of Computational Physics, **227** (2008), pp. 4089-4122.

[9] P. L. Roe, *Approximate Riemann solvers, parameter vectors and difference scheme*, Journal of Computational Physics, **43 (**1981), pp. 357-372.

[10] K. Kim, C. Kim, and O. Rho, *Methods for the accurate computations of hypersonic flows, Part I: AUSMPW+ scheme*, Journal of Computational Physics, **174** (2001), pp. 38-80.

[11] K. Kim, and C. Kim, *Accurate, Efficient and Monotonic Numerical Methods for Multi-dimensional Compressible Flows Part I: Spatial Discretization*, Journal of Computational Physics, **208** (2005), pp. 527-569.
[12] C. W. Shu and S. Osher, *Efficient implementation of essentially non-oscillatory shock-capturing schemes*, Journal of Computational Physics, **77** (1988), pp. 439-471.